

Author's Accepted Manuscript

Temporally correlated fluctuations drive
epileptiform dynamics

Maciej Jedynek, Antonio J. Pons, Jordi Garcia-
Ojalvo, Marc Goodfellow



PII: S1053-8119(16)30652-8
DOI: <http://dx.doi.org/10.1016/j.neuroimage.2016.11.034>
Reference: YNIMG13582

To appear in: *NeuroImage*

Received date: 14 July 2016
Accepted date: 13 November 2016

Cite this article as: Maciej Jedynek, Antonio J. Pons, Jordi Garcia-Ojalvo and Marc Goodfellow, Temporally correlated fluctuations drive epileptiform dynamics, *NeuroImage*, <http://dx.doi.org/10.1016/j.neuroimage.2016.11.034>

This is a PDF file of an unedited manuscript that has been accepted for publication. As a service to our customers we are providing this early version of the manuscript. The manuscript will undergo copyediting, typesetting, and review of the resulting galley proof before it is published in its final citable form. Please note that during the production process errors may be discovered which could affect the content, and all legal disclaimers that apply to the journal pertain.

Temporally correlated fluctuations drive epileptiform dynamics

Maciej Jedynek^{a,b,*}, Antonio J. Pons^a, Jordi Garcia-Ojalvo^b, Marc Goodfellow^{c,d,e}

^a*Departament de Física i Enginyeria Nuclear, Universitat Politècnica de Catalunya, Terrassa, Spain.*

^b*Department of Experimental and Health Sciences, Universitat Pompeu Fabra, Parc de Recerca Biomèdica de Barcelona, Barcelona, Spain.*

^c*College of Engineering, Mathematics and Physical Sciences, University of Exeter, Exeter, UK.*

^d*Centre for Biomedical Modelling and Analysis, University of Exeter, Exeter, UK.*

^e*EPSRC Centre for Predictive Modelling in Healthcare, University of Exeter, Exeter, UK.*

Abstract

Macroscopic models of brain networks typically incorporate assumptions regarding the characteristics of afferent noise, which is used to represent input from distal brain regions or ongoing fluctuations in non-modelled parts of the brain. Such inputs are often modelled by Gaussian white noise which has a flat power spectrum. In contrast, macroscopic fluctuations in the brain typically follow a $1/f^b$ spectrum. It is therefore important to understand the effect on brain dynamics of deviations from the assumption of white noise. In particular, we wish to understand the role that noise might play in eliciting aberrant rhythms in the epileptic brain.

To address this question we study the response of a neural mass model to driving by stochastic, temporally correlated input. We characterise the model in terms of whether it generates “healthy” or “epileptiform” dynamics and observe which of these dynamics predominate under different choices of temporal correlation and amplitude of an Ornstein-Uhlenbeck process. We find that certain temporal correlations are prone to eliciting epileptiform dynamics, and that these correlations produce noise with maximal power in the δ and θ bands.

*Corresponding author

Email address: maciej.jedynek@protonmail.com (Maciej Jedynek)

Crucially, these are rhythms that are found to be enhanced prior to seizures in humans and animal models of epilepsy. In order to understand why these rhythms can generate epileptiform dynamics, we analyse the response of the model to sinusoidal driving and explain how the bifurcation structure of the model gives rise to these findings. Our results provide insight into how ongoing fluctuations in brain dynamics can facilitate the onset and propagation of epileptiform rhythms in brain networks. Furthermore, we highlight the need to combine large-scale models with noise of a variety of different types in order to understand brain (dys-)function.

Keywords: Epilepsy, Ictogenesis, Neural Mass Models, Jansen-Rit Model, Nonlinear Dynamics, Stochastic Effects, Ornstein-Uhlenbeck Noise.

1. Introduction

Epilepsy is a prevalent neurological disorder characterised by the recurrence of spontaneous seizures. Seizures predominantly arise amidst a backdrop of otherwise healthy brain activity and are often accompanied by salient changes in electrographic activity as measured, for example, on the electroencephalogram (EEG). There is much we do not understand about why seizures occur, and contributing factors exist across multiple temporal and spatial scales [1, 2]. Here we focus upon a large spatial scale of interconnected brain regions since this is the scale at which clinical signs and symptoms emerge, and clinical data are most often recorded. At this scale, deficits can be observed both in the dynamics of brain regions [3, 4] and the connections between brain regions [5]. Thus recent focus has been placed on the role that large-scale brain networks play in epilepsy [6, 7, 8, 9]. A fundamental, unanswered question in this context is how seizures emerge and spread in such networks [10, 11, 12, 13, 14, 15].

Understanding seizures as emergent dynamics in brain networks is a challenging endeavour. However, mathematical models of brain dynamics can be used to study the mechanisms underlying the generation of seizures [16, 1, 2]. Previous work has focused on the types of dynamics that could underpin tran-

sitions from healthy EEG to seizure EEG, such as changes in model parameters
 20 (bifurcations), co-existence of healthy and abnormal states (bistability) or more
 complex spatiotemporal dynamics [17, 18, 19, 10, 20, 21, 22]. The bifurcation
 route into seizures relies on a (relatively) slow time scale change in the brain that
 drives it into an alternate (pathological) state, whereas the bistability paradigm
 relies on a (fast) perturbation-induced transition from the healthy to patholog-
 25 ical state. However, any of these scenarios can be assumed to occur amidst a
 backdrop of ongoing brain dynamics, which could additionally influence transi-
 tions into seizures.

Modelling studies of seizure onset typically lump the “background” dynam-
 ics of the brain into stochastic fluctuations. These fluctuations have most of-
 30 ten been assumed to have a flat power spectrum (i.e. Gaussian white noise)
 [23, 24, 25, 26, 27, 12, 28], which can be motivated by the assumption that
 ongoing activity of the brain is so complex that no single frequency dominates.
 However, analysis of spectra of brain signals (for example scalp EEG) reveals on-
 going brain dynamics to be characterised by a $1/f^b$ relationship [29], with promi-
 35 nent frequencies appearing concomitantly with different brain states [30, 29, 31].
 In the epileptic brain, abnormal (“epileptiform”) rhythms such as spikes or slow
 waves can also be present, even during interictal periods [32, 33]. In particular,
 in humans an increase of power in the delta band has been observed in MEG
 [34] and EEG [35] recordings preceding absence seizures and pathological slow
 40 rhythms can be observed in interictal or preictal periods associated with focal
 epilepsies [32, 36, 37]. In animal models of epilepsy, electrophysiological record-
 ings performed in the preictal phase have revealed an increase of power in the
 delta [38], and delta and theta [39] bands.

We therefore need to better understand the response of neuronal populations
 45 to afferent rhythms and stochastic fluctuations with a variety of dynamics, in-
 cluding those that can be approximated by noise yielding a realistic $1/f^b$ power
 spectrum, and those that contain dominant rhythms observed in the epilep-
 tic brain. A natural choice for the generation of such noise is the Ornstein-
 Uhlenbeck (OU) process, which exhibits a Lorentzian power spectrum. The

50 spectral distribution in the OU process can be tuned through temporal correlations (i.e. “colour”) of the resulting noise, therefore modelling alternative spectral compositions. OU noise has also been associated with the integration of background synaptic activity acting upon a neuron [40]. Recent studies of OU processes driving neural models have investigated the effects of coloured
55 noise on temporal distributions of neuronal spiking [41, 42] and the generation of multimodal patterns of alpha activity [43]. In addition, networks of spiking neurons [44] and of neuronal populations [45] have been shown to generate realistic $1/f^b$ -like spectra when driven by OU noise, or more complex dynamics when subjected to driving at specific frequencies [46, 47]. However, we lack an
60 understanding of the ways in which non-white noise or rhythmic perturbations interact with neuronal populations to produce epileptiform dynamics.

Here, we study the effect of temporally correlated noise and rhythmic driving on the generation of epileptiform dynamics. Our starting point is a neural mass model that represents canonical interactions between populations of neurons in a
65 region of brain tissue. Such models have been shown to be capable of generating pathological spiking dynamics reminiscent of seizure activity [48, 49, 50, 51]. We classify the dynamics of this model by assessing variations of the signal around its time-averaged value, thus distinguishing between “healthy” and epileptiform dynamics. We then study the response of the system to prototypical coloured
70 noise (an OU process) and identify an interval of temporal correlations for which noise can more readily elicit epileptiform dynamics. We show that this region is bounded on the one hand by noise intensity being insufficient to generate spikes, and on the other by bursting and transitions to an alternative rhythmic state, previously used to model healthy dynamics (the alpha rhythm). Analysing
75 the spectrum of noise in this interval reveals it to contain high power in low (2-8 Hz) frequencies. In order to understand why such frequencies can drive epileptiform rhythms, we study periodic perturbations in a deterministic version of the model. Our analysis shows that driving the deterministic model using frequencies in this band causes epileptiform dynamics to predominate. We show
80 how consideration of the bifurcation structure of the model can shed light on

these observations, which in turn highlight the need to consider a fuller analysis of the repertoire of dynamics in the model beyond the genesis of epileptiform rhythms. Our findings elucidate potential mechanisms by which healthy or epileptiform rhythms present in certain regions of the brain can cause the onset
 85 of aberrant dynamics in connected regions.

2. Materials and methods

2.1. Jansen and Rit model

In order to study the dynamics of regions of brain tissue, we use a neural mass model of a canonical circuit of interacting neuronal populations [48, 49].
 90 The populations considered are pyramidal neurons, excitatory interneurons and inhibitory interneurons. The dynamics of these populations is governed by a linear transformation that converts presynaptic spiking activity to changes in postsynaptic membrane potential (PSP) and a nonlinear transformation of net membrane potential to an efferent firing rate.

The linear transformation is given by the following convolution:

$$y(t) = \int_{-\infty}^t h(t') s_{\text{in}}(t - t') dt', \quad (1)$$

95 where $s_{\text{in}}(t)$ is the spike rate of activity afferent to the population, $y(t)$ gives the dynamics of the PSP, and $h(t)$ describes the way in which membrane potentials respond to an activating impulse. $h(t)$ equals zero for $t < 0$ and otherwise is given for excitatory and inhibitory connections with the following equations:

$$h_e(t) = Aate^{-at}, \quad (2)$$

$$h_i(t) = Bbte^{-bt}, \quad (3)$$

where A and B are the maximum excitatory and inhibitory PSPs, respectively,
 100 and a and b are time constants of these responses. They follow from lumped contributions of all dilatory effects that include synaptic kinetics, dendritic signal propagation and leak currents [52, 53, 54, 55, 23].

Eq. 1 can be rewritten, using Eq.2, as a second order ordinary differential equation (ODE):

$$\frac{d^2y(t)}{dt^2} + 2a\frac{dy(t)}{dt} + a^2y(t) = Aa \cdot s_{in}(t), \quad (4)$$

105 Similarly, by using Eq. 3 one can find a corresponding representation for inhibitory population dynamics.

Conversion of net membrane potential to efferent spiking is given by the following sigmoid function:

$$s_{out}(y) = \text{Sigm}(y) = \frac{2e_0}{1 + e^{r(\nu_0 - y)}}, \quad (5)$$

where $s_{out}(y)$ is a firing rate of a spike train outgoing from the population, y is its momentary total PSP (in general, time dependent), $2e_0$ is the maximum firing rate, ν_0 is the PSP for which half maximum of the firing rate is reached, 110 and r determines steepness (and thus nonlinearity) of this transformation.

The two described transformations allow to model circuits of interconnected neuronal populations. A circuit corresponding to a Jansen-Rit model of a cortical column is shown in black in Fig. 1.

The equations above lead to a full description of circuit dynamics (Fig. 1) 115 as follows:

$$\begin{cases} \ddot{y}_0(t) + 2a\dot{y}_0(t) + a^2y_0(t) = Aa \text{ Sigm}[y_1(t) - y_2(t)] & (6) \end{cases}$$

$$\begin{cases} \ddot{y}_1(t) + 2a\dot{y}_1(t) + a^2y_1(t) = Aa\{I_{ex}(t) + C_2 \text{ Sigm}[C_1y_0(t)]\} & (7) \end{cases}$$

$$\begin{cases} \ddot{y}_2(t) + 2b\dot{y}_2(t) + b^2y_2(t) = Bb\{C_4 \text{ Sigm}[C_3y_0(t)]\} & (8) \end{cases}$$

where y_0 is proportional to excitatory PSPs induced on both populations of interneurons, y_1 is a net excitatory PSP induced on the population of pyramidal neurons and y_2 is an inhibitory PSP on this population. Subsequently $y_1 - y_2$ is the resultant PSP on this population, which following previous studies 120 is assumed to be proportional to the measured EEG. We set parameters of the neural mass model to typically used values as given in [49]: $e_0 = 2.5 \text{ s}^{-1}$,

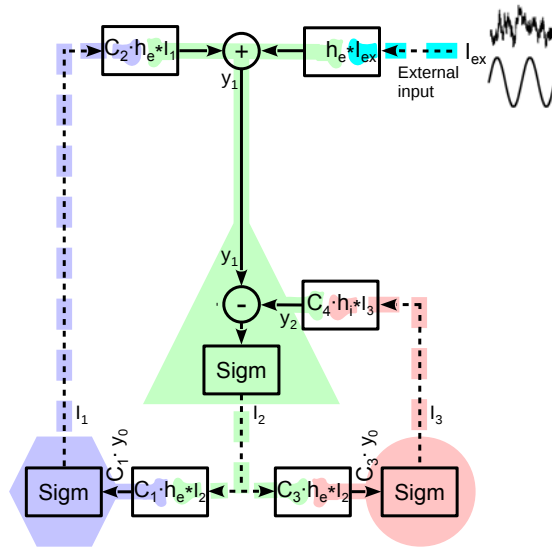


Figure 1: A scheme of the Jansen-Rit model of a cortical column that comprises three neuronal populations. A population of pyramidal neurons is marked with green, and populations of excitatory and inhibitory interneurons with blue and red, respectively. Somata are depicted with the triangle, hexagon and circle. Continuous lines stand for dendritic processing and dashed ones for axonal processing. A dot means multiplication and a star operator denotes convolution. Cyan indicates lumped external input from sub-cortical and cortico-cortical structures. The black circuit depicts an analytic description of the underlying structure of a cortical column. See text for details.

$v_0 = 6 \text{ mV}$, $r = 0.56 \text{ mV}^{-1}$, $A = 3.25 \text{ mV}$, $B = 22 \text{ mV}$, $a = 100 \text{ s}^{-1}$, $b = 50 \text{ s}^{-1}$,
 $C_1 = 135$, $C_2 = 108$, $C_3 = C_4 = 33.75$.

2.2. Driving of the model

$I_{\text{ex}}(t)$ in Eq. 7 represents external input to the microcircuit, lumping together
 125 cortico-cortical and sub-cortical afferents. The effect of $I_{\text{ex}}(t)$ on the dynamics
 of the model is the focus of our study. Previous studies have sought to under-
 stand the dynamics of the model by examining the effect of I_{ex} as a bifurcation
 parameter and found certain values of this parameter to lead to epileptiform
 130 spiking [49, 51, 46, 27]. In Fig. 2 we recreate with XPPAUT [56] the results
 of [51], illustrating the invariant sets of the model that exist for different, time
 invariant values of I_{ex} . To ease subsequent interpretations of dynamics invoked
 by different choices of temporally varying $I_{\text{ex}}(t)$, we briefly review the different
 dynamic regimes that are possible in this model. Although in Fig. 2 we plot
 135 a range of I_{ex} that includes negative values (region I in Fig. 2), we focus on
 positive values of I_{ex} , since only these are biologically plausible. The regime
 marked II in Fig. 2 spans for $-12.15 \text{ s}^{-1} < p < 89.83 \text{ s}^{-1}$. It is a bistable
 regime that contains two stable fixed points: a node (blue) and a focus (cyan).
 At $p = 89.83 \text{ s}^{-1}$ the focus transitions to a limit cycle (green) in a supercriti-
 140 cal Hopf bifurcation. This limit cycle has its characteristic frequency close to
 10 Hz, and has therefore previously been used to model the alpha rhythm of the
 brain (henceforth referred to as “alpha limit cycle”). The regime marked III is
 also bistable, however here the two stable solutions are the node (blue) and the
 alpha limit cycle (green). At $p = 113.58 \text{ s}^{-1}$ the stable node ceases to exist in
 145 a saddle-node on invariant circle (SNIC) bifurcation that creates a limit cycle
 reminiscent of epileptiform spikes, henceforth referred to as “epileptiform limit
 cycle” (continuous red line, Fig. 2). The frequency of this limit cycle ranges
 from 0 Hz at its creation to $\sim 5 \text{ Hz}$ at its termination point. Region IV in Fig. 2
 denotes a bistable regime in which the epileptiform limit cycle coexists with the
 150 alpha limit cycle. Regime V starts at $p = 137.38 \text{ s}^{-1}$, where the epileptiform
 limit cycle vanishes in a fold of limit cycles. In regime V the alpha limit cycle

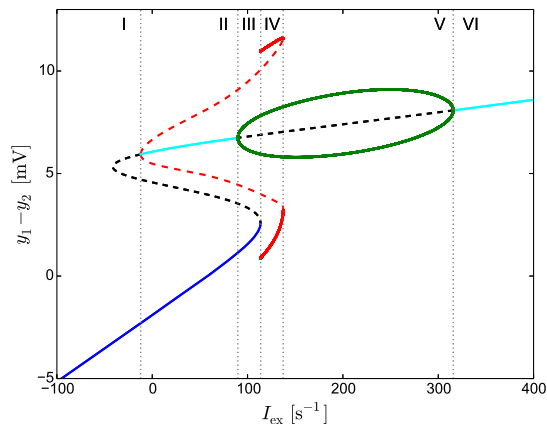


Figure 2: Bifurcation diagram of the Jansen-Rit model defined in Eqs 6-8. Parameters of the model were set to biologically plausible values proposed in [49]. The X axis shows external, constant input to the pyramidal population $I_{\text{ex}} = p$. The Y axis shows net postsynaptic potential on this population: $y_1 - y_2$. Continuous (dashed) lines represent stable (unstable) solutions. Cyan and blue denote a node and a focus, respectively, and green and red indicate alpha and epileptiform limit cycles, respectively. Vertical, grey dotted lines divide the diagram to six regimes (denoted by roman numerals) of qualitatively distinct dynamical properties. See text for details.

is the only stable solution. It ceases to exist in a supercritical Hopf bifurcation at $p = 315.70 \text{ s}^{-1}$, where the last regime, marked with VI, starts. The focus (cyan) remains the only stable solution there.

Here we focus on the dynamics of the microcircuit under the influence of noisy or rhythmic perturbations from other regions of the brain. We therefore decompose $I_{\text{ex}}(t)$ into a time invariant part p and a zero-mean, time dependent component $u(t)$ as follows:

$$I_{\text{ex}}(t) = p + u(t) \quad (9)$$

p determines the average working point of the system in the landscape of dynamical regimes as shown in Fig. 2. Following from our previous study [45] we choose a default value of $p = 89 \text{ s}^{-1}$, placing the system close to the Hopf bifurcation. $u(t)$ represents deterministic or stochastic perturbations: for the former, we use $u(t) = \tilde{A} \sin(\frac{2\pi}{T}t + \phi)$, for the latter, we use an Ornstein-Uhlenbeck (OU)

process. This noise, ξ_{ou} , is derived from the solution of the following linear stochastic differential equation:

$$\frac{d\xi_{\text{ou}}}{dt} = -\frac{\xi_{\text{ou}}}{\tau} + \frac{\sqrt{2D}}{\tau}\xi_w(t) \quad (10)$$

where $\xi_w(t)$ is a random variable representing Gaussian white noise with zero mean and correlation $\langle \xi_w(t)\xi_w(t') \rangle = \delta(t-t')$ and τ is correlation time of the OU noise. The standard deviation of this noise in the steady state is:

$$\sigma_{\text{ou}} = \sqrt{\frac{D}{\tau}} \quad (11)$$

The variables I_{ex} , p , u , $\xi_{\text{ou}}(t)$ and σ_{ou} represent firing rates of spike trains and therefore are expressed in s^{-1} . The intensity of the noise can be defined as the product of its stationary variance (accounting for amplitudes of random fluctuations) and its correlation time (accounting for persistence of the fluctuations) [57]. In the notation adopted here, the intensity defined in this way is given by D . Finally, the power spectrum of the OU noise is given by the Lorentzian function:

$$S_{\text{ou}}(f) = \frac{2D}{1 + 4\pi^2\tau^2 f^2} \quad (12)$$

155 In order to study how the frequency content of OU noise relates to traditionally defined EEG frequency bands (i.e. $\delta, \theta, \alpha, \beta, \gamma$) we quantify the fraction of total spectral power of the noise (characterised with correlation time τ) contained in a certain frequency window, bounded by $f_{\text{min}}, f_{\text{max}}$:

$$E(\tau, f_{\text{min}}, f_{\text{max}}) = \frac{2}{P_{\text{tot}}} \cdot \int_{f_{\text{min}}}^{f_{\text{max}}} S_{\text{ou}}(f)df = \frac{2}{\pi} \arctan(2\pi\tau f) \Big|_{f_{\text{min}}}^{f_{\text{max}}} \quad (13)$$

160 where the normalisation factor P_{tot} yields the total power and equals $\int_{-\infty}^{\infty} S_{\text{OU}}(f)df = \frac{D}{\tau}$. The factor 2 in front of the integral follows from taking into account power transmitted in both the positive and negative frequency bands.

2.3. Classification of model dynamics

As previously described [49, 51, 58, 27], the model can display “healthy” or “epileptiform” rhythms depending upon its parametrisation and the nature of

165 its input, I_{ex} (see Eq.9). By considering the bifurcation diagram shown in Fig. 2,
 we define epileptiform dynamics as those corresponding to the epileptiform limit
 cycle, and healthy dynamics as any of the other regimes. The latter comprises
 either noise-driven fluctuations around the node, or oscillations with frequency
 close to 10Hz (alpha oscillations) due to the presence of, or proximity to, the
 170 limit cycle generated by the Hopf bifurcation.

Our classification of the output of the Jansen-Rit cortical column in these
 three categories is depicted in Fig. 3. The classification is established via the
 following algorithm: first, a moving average of the model's output $y_1 - y_2$ is
 computed with a sliding window of length 0.4 s. This window is long enough
 175 to sufficiently smooth out the signal (see Fig. 3B) and thus allow for estimation
 of its variability (details below), and short enough to mark transitions between
 dynamical regimes with good temporal accuracy (see Fig. 3A).

Second, the root mean square ($\text{RMS}_{(y_1 - y_2)}$) of the $y_1 - y_2$ signal around
 this mean is obtained. When this quantity is high, variations of the signal are
 180 rapid and/or have a high-amplitude, which are features of the epileptiform limit
 cycle. Therefore, we set a threshold $\text{Th}_B = 2.25$ mV (dashed line in Fig. 3C)
 that establishes the value of $\text{RMS}_{(y_1 - y_2)}$ above which a specific time point of the
 signal is classified as being in epileptiform dynamics. Otherwise, we compare
 the smoothed $y_1 - y_2$ signal with the threshold value $\text{Th}_A = 5$ mV (dashed line
 185 in Fig. 3B), which separates the focus from the node along the $y_1 - y_2$ axis (c.f.
 Fig.2). If the smoothed signal is greater than Th_A , we classify a data point
 as alpha oscillations, if it is smaller, we classify it as noisy fluctuations around
 the node. Note that this methodology is valid also for deterministic conditions,
 as in Sec. 3.3. The thresholds Th_A and Th_B as well as the window length
 190 have been set such that resulting classification complies with inspection by eye.
 The attractor-based classification method described above is adequate in our
 case, since our model attractors can be sufficiently distinguished by amplitude.
 For other types of models, or for the analysis of experimental data, adding
 frequency information to aid the classification might be beneficial, although
 195 purely temporal classifications have been found to be sufficient in some cases

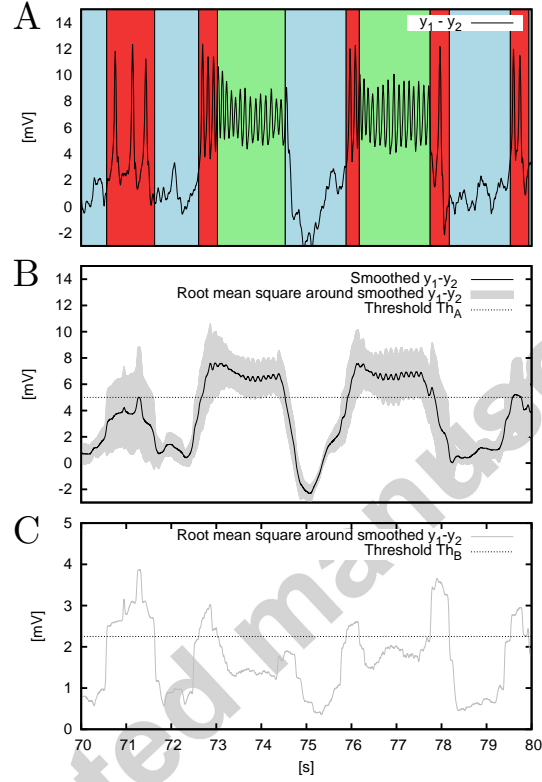


Figure 3: Methodology for classification of dynamics. Panel A shows $y_1 - y_2$ obtained from 10 seconds of stochastic simulation for $p = 89 \text{ s}^{-1}$, $\tau = 10^{-0.5} \text{ s}$, $\sigma_{ou} = 50 \text{ s}^{-1}$. Background colours indicate the type of activity assigned with the classification algorithm. Red stands for epileptiform dynamics, green for alpha oscillations, and blue for random fluctuations around the node. Panel B shows a smoothed version of the $y_1 - y_2$ signal from panel A, obtained with a running mean computed within a 0.4-second-long sliding window. The dashed line denotes the $Th_A = 5 \text{ mV}$ threshold, which is used to discriminate between stochastic fluctuations around the node (smoothed $y_1 - y_2 \leq Th_A$) and alpha oscillations (smoothed $y_1 - y_2 > Th_A$). Grey marks root mean square of $y_1 - y_2$ around its smoothed version ($RMS_{(y_1 - y_2)}$). This value is shown in panel C in grey along with the $Th_B = 2.25 \text{ mV}$ threshold, which is used to identify epileptiform dynamics (when $RMS_{(y_1 - y_2)} > Th_B$).

[59].

2.4. Computational simulation

We integrated the system using the stochastic Heun scheme [60] with a time step equal to 10^{-4} s, and we stored every tenth point of the simulation. For each value of noise correlation time τ and stationary standard deviation σ_{ou} we performed 10 simulations, each with different realisation of the noise and we averaged the results. Each simulation was 111 seconds long. The first 10 seconds were discarded and one second buffered the sliding window. In the deterministic system, the model was simulated for 111 seconds, with 100 seconds of transient discarded and one second buffering the sliding window. This means that the effective time courses used in the deterministic analysis were 10 seconds long, which corresponds to the longest period of the driving sinusoid that we utilised.

3. Results

3.1. Noise induced epileptiform dynamics

Simulations of the model under different values of the correlation time, τ , of the driving Ornstein-Uhlenbeck (OU) noise reveal qualitatively different dynamics (Fig. 4). For weakly correlated noise (low values of τ) stochastic fluctuations around the node predominate (Fig. 4A). For intermediate temporal correlations epileptiform rhythms are more often observed (Fig. 4B), whilst at larger correlation times the model displays mainly node and alpha activities (Fig. 4C). These results suggest that epileptiform dynamics are more readily observed for noise with intermediate correlation times. In order to systematically study this effect, simulations of the model were performed for different values of τ and standard deviation of the noise, σ_{ou} . For each simulation, we measured the fraction of the total time that the system spent in epileptiform dynamics (Fig. 4D).

Fig. 4D shows that for large enough values of the standard deviation σ_{ou} epileptiform dynamics arise for an intermediate value of the noise correlation time. As σ_{ou} decreases, the interval of values of τ for which epileptiform dynamics predominates is shifted to larger values. The intensity of OU noise, D , as

225 described in Eq. 11 is overlaid in white dashed lines on Fig. 4D. It can be seen
 that the onset of epileptiform dynamics for intermediate values of τ coincides
 with constant values of D . This means that in order to generate epileptiform dy-
 namics, the noise generated by the OU process should have sufficient intensity,
 regardless of its power and correlation time. However, this simple relationship
 230 does not hold for $\tau \gtrsim 10^{-1.5}$ s. The system more often displays alpha oscilla-
 tions for large correlation times ($\tau \gtrsim 10^{-0.5}$ s) than for small correlation times.
 Supplementary Fig. S1 illustrates the fractions of time that the system spends
 in alpha oscillations and in the node attractor. In order to test the generalis-
 ability of these results, we performed equivalent simulations under alternative
 235 choices of parameters a and b , such that the presence of the attractor repre-
 senting epileptiform dynamics was preserved. We found that although changes
 in the bifurcation diagram occurred (Fig. S2 in Supplementary Materials), the
 value of τ maximising the presence of epileptiform dynamics remained the same
 (Fig. S3 in Supplementary Materials). Increasing the value of σ still further can
 240 be seen to increase the range of τ over which epileptiform dynamics are elicited
 (Fig. S4 in Supplementary Materials).

3.2. Relationship to brain rhythms

To relate these findings to underlying frequency components of brain rhythms
 we studied how OU processes with different correlation times distribute their
 245 power in different frequencies. In order to do this we used Eq. 13 to quantify the
 fraction of power deposited by the noise (characterised with correlation time, τ)
 in a given frequency window (f_{\min}, f_{\max}). Evaluation of this function for f_{\min}
 and f_{\max} set according to boundaries of traditionally defined EEG frequency
 bands ($\delta, \theta, \alpha, \beta, \gamma$) is shown in Fig. 5. For each frequency band, the location of
 250 the maximum of the E function (Eq.13) represents the value of noise correlation
 time τ that maximises spectral power of the noise within that band. Values
 of τ corresponding to these maxima are indicated with coloured circles on the
 X axis of Fig.5. They demonstrate that the choice of noise correlation time
 $\tau = 10^{-1.55}$ s maximises spectral power in the θ band (cyan). Furthermore,

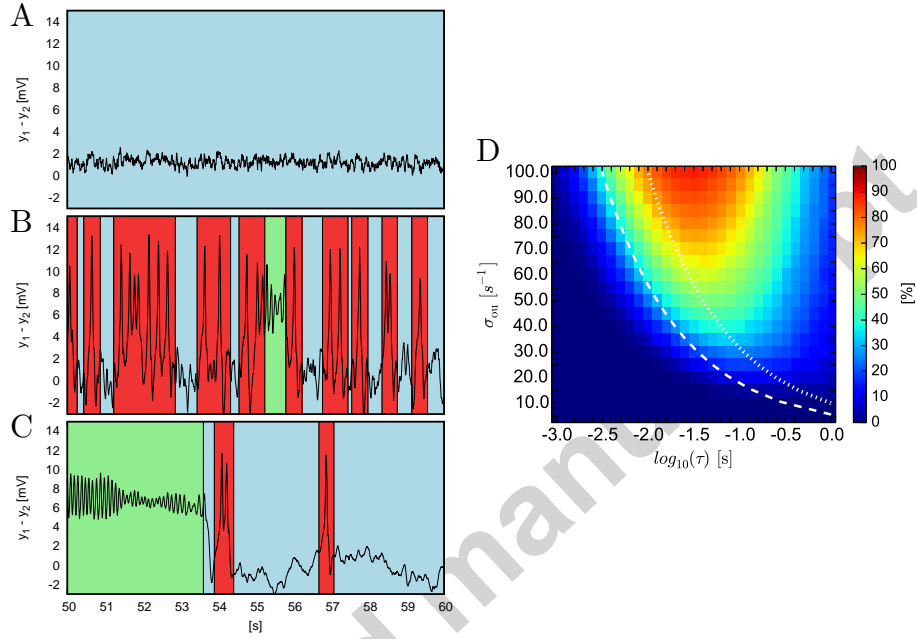


Figure 4: Response of the Jansen-Rit model to driving with the Ornstein-Uhlenbeck (OU) noise. The left panels of the figure show example outputs (time courses of $y_1 - y_2$) produced by the model under driving with the OU noise characterised with correlation time τ equal to 10^{-3} s (panel A), $10^{-1.5}$ s (panel B) and 10^0 s (panel C). Background colours mark periods of random fluctuations around the node (blue), epileptiform dynamics (red) and alpha activity (green). In all these cases stationary standard deviation of the noise σ_{ou} was equal to 50 s^{-1} and p was set to 89 s^{-1} . Panel D shows the fraction of time that the system spent in epileptiform dynamics as a function of the noise correlation time τ (varied along the X axis in logarithmic scale) and the noise stationary standard deviation σ_{ou} (varied along the Y axis). Locations of the red letters A,B and C mark settings in which time traces shown in panels A,B and C were obtained. The white lines denote points of equal values of noise intensity D : the dashed line marks $D = \sqrt{1000} \text{ s}^{-1}$ and the dotted one marks $D = 100 \text{ s}^{-1}$. In all cases initial conditions corresponded exactly to the node.

255 $\tau = 10^{-1.25}$ maximises spectral power in the δ band (magenta). Experimental studies suggest that enhancement of rhythms falling to these two bands may precede occurrence of epileptiform activity [34, 35, 39, 38]. We therefore combine δ and θ bands together and find that spectral power within this $\delta+\theta$ band is maximised for $\tau = 10^{-1.4}$. As shown in the previous section (Fig. 4), this value of τ coincides with correlation times of the driving noise for which epileptic spiking is most prevalent. Therefore, we speculate that rhythms around the θ band (4-8Hz) or in the wider $\delta + \theta$ band (2-8Hz) are particularly prone to eliciting epileptiform dynamics in the model.

3.3. Periodic driving in the deterministic system

265 In order to test this prediction, we analysed the response of the system to harmonic driving $u(t) = \tilde{A} \sin(\frac{2\pi}{T}t + \phi)$. We systematically varied the amplitude \tilde{A} , period T and phase ϕ of the harmonic driving, and quantified the dynamics of the model. It has previously been shown that the Jansen-Rit model displays a variety of dynamics, caused by rhythmic driving, including periodicity, quasi-periodicity and chaos [47, 46]. In this case, however, we narrow our interest to whether the activity resembles epileptiform dynamics, alpha oscillations, or fluctuations around the node, and therefore apply the same classification algorithm as in the stochastic system (see Methods and Fig.3). We focus on elucidating values of amplitude and frequency for which healthy or epileptiform dynamics are observed.

275 Fig. 6 shows the presence of each of these dynamics when the amplitude and period of the driving harmonic signal are varied. Alpha oscillations and the node solution are encoded with oblique stripes (top-right to bottom-left for the node and top-left to bottom-right for alpha) and epileptiform dynamics are encoded with grey. Fig. 6A corresponds to settings where initial conditions were set exactly to the node, whereas Fig. 6B corresponds to initial conditions exactly at the focus. Fig. 6A demonstrates that for fast periodic driving ($T \lesssim 10^{-0.8}$ s), the initial node dynamics are preserved and epileptiform rhythms are not elicited even when the driving amplitude is large. On the other hand, for very slow driv-

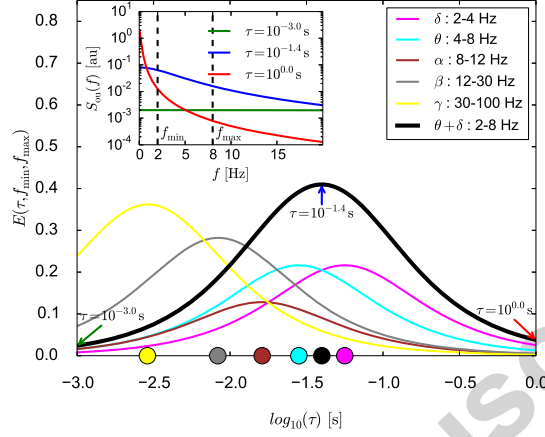


Figure 5: Distribution of spectral power in frequency bands of standard brain rhythms and dependence of location of maximum power on noise correlation time τ . Evaluation of the $E(\tau, f_{\min}, f_{\max})$ function (see Eq. 13) of an Ornstein-Uhlenbeck noise characterised with correlation time τ within a frequency range f_{\min}, f_{\max} is plotted for fixed frequency ranges that correspond to distinct brain rhythms: δ (2-4 Hz, magenta), θ (4-8 Hz, cyan), α (8-12 Hz, brown), β (12-30 Hz, grey), γ (30-100 Hz, yellow) and combined $\delta + \theta$ (2-8 Hz, black). Units on the Y axis express fraction of the spectral power of the noise characterised with τ contained within the f_{\min}, f_{\max} range. Correlation time of the noise τ varies along the X axis. The inset illustrates the meaning of $E(\tau, f_{\min}, f_{\max})$. It shows an example theoretical power spectrum of the Ornstein-Uhlenbeck noise calculated for $\tau = 10^{-3.0}$ s (green), $\tau = 10^{-1.4}$ s (blue) and $\tau = 10^0$ s (red). In each case stationary variance $\frac{D}{\tau}$ was set to an arbitrary value 1 s^{-2} . Dashed vertical lines mark the $f_{\min} = 2$ Hz, $f_{\max} = 8$ Hz range, for which the black plot shown in the main panel was derived from Eq. 13. Green, blue and red arrows on the main plot indicate values of the $E(\tau, f_{\min}, f_{\max})$ function that correspond to these spectra. The value indicated by the blue arrow is highest (in this case it corresponds to the maximum), which follows from the fact that the area below the blue curve, limited by f_{\min} and f_{\max} in the inset is greater than area set by either red, or green curves. Coloured circles on the X axis indicate values of τ corresponding to maxima of $E(\tau, f_{\min}, f_{\max})$: $\tau = 10^{-2.54}$ s for γ , $\tau = 10^{-2.08}$ s for β , $\tau = 10^{-1.79}$ s for α , $\tau = 10^{-1.55}$ s for θ , $\tau = 10^{-1.25}$ s for δ , and $\tau = 10^{-1.4}$ s for $\delta + \theta$.

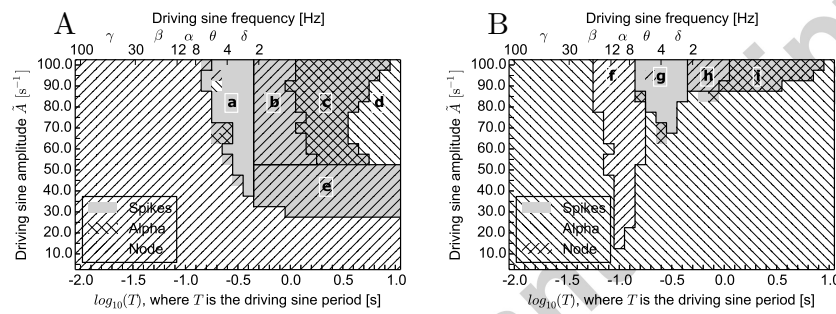


Figure 6: Phase diagram showing the different dynamical regimes resulting from oscillatory driving with varying amplitude and period. The response of the Jansen-Rit model under harmonic driving was classified as either a node (oblique stripes from top-right to bottom-left), alpha activity (oblique stripes from top-left to bottom-right), or epileptiform dynamics (grey). This classification was conducted for varying driving amplitude \tilde{A} , displayed on Y axes, and driving period T , displayed on X axes in logarithmic (bottom) and linear (top) scales. Ranges and names of typical brain rhythms are denoted on the linear scale. In general, different dynamical regimes might coexist, therefore patterns overlap. Panel A corresponds to initial conditions set exactly to the node and panel B to initial conditions set exactly to alpha oscillations. In both cases $p=89 \text{ s}^{-1}$. Black lines divide the diagram into distinct regimes, annotated with letters.

285 ing ($T > 10^{0.5}$ s) and sufficiently high amplitude ($\tilde{A} > 50$ s $^{-1}$), alpha oscillations dominate (regime “d”). Similarly to the stochastic case, epileptiform dynamics prevail for intermediate periods of the driving and sufficiently large amplitude (regime “a”). An exemplary time course corresponding to this case is provided in supplementary Fig. S5. For initial conditions set to alpha oscillations, Fig. 6B
 290 demonstrates that neither fast ($T \lesssim 10^{-1.2}$ s) nor slow driving, characterised with an amplitude not exceeding a limit value, causes transitions away from the initial dynamics. Similarly to the node initial conditions, intermediate values of τ give rise to epileptiform dynamics (regime “g”). In particular, exclusively epileptiform dynamics occur when driving frequencies correspond to either δ or
 295 θ rhythms.

Driving with frequencies of ~ 10 Hz leads to a resonance effect, causing an escape from alpha oscillations to the node. This effect is present in regime “f” and the corresponding time course is shown in Fig. S6, in Supplementary Materials. This resonance results in long-term node dynamics. However, when
 300 excitability of the model is increased (an increase in parameter p), this escape from the alpha attractor is followed by epileptic activity (see Supplementary Fig. S7). Figs 6A and B were obtained for $\phi = 0$. We note that alternative choices of ϕ did not alter the results of Fig. 6A. However, we did identify an effect of altering phase in that the resonance regime (“f” in Fig. 6B) is slightly
 305 narrower when the driving sinusoid is shifted by the phase $\phi = +\frac{\pi}{2}$. In these conditions no resonance appears for $T = 10^{-1.2}$ s, and for $T = 10^{-1.1}$ s and $\tilde{A} \in [70$ s $^{-1}$, 85 s $^{-1}]$. For other phase shifts this effect of resonance attenuation is not prominent, or does not occur, but the lower boundaries of regimes “g”, “h” and “i” can be extended towards smaller values of \tilde{A} for some non-zero
 310 phase shifts.

These effects can be understood from the structure of the bifurcation diagram of the model [51] shown in Fig. 2. In particular, transient periods of intensive spiking (bursting), interleaved with periods of quiescence are observed when a slowly varying input periodically crosses the bifurcation and leads the system
 315 to alternate between regimes III and IV. In this case, the system switches be-

tween the node (denoted by blue in regime III in Fig. 2) and epileptiform spikes (continuous red in regime IV). These dynamics are represented in Fig. 6 as combined spiking+node activity in regimes “b” and “h”. In this case, although the driving amplitudes can be high enough to enter regime V, alpha oscillations are not observed, because driving is too fast and the system does not have time to converge to these oscillations. Furthermore, regime “e” in Fig. 6A marks driving that is slow enough and characterised by amplitudes high enough to cross the excitability threshold (enter regime IV in Fig. 2) - thus eliciting bursts of spikes - but at the same time not large enough to enter regime V of alpha oscillations. An exemplary bursting time course, corresponding to this regime is provided in Supplementary Materials, in Fig. S8.

Slow driving with sufficiently high amplitude moves the system through all dynamic regimes and overshoots the epileptiform spiking regime to regime V where alpha oscillations are the only existing dynamics. In this case, the system displays the effects of hysteresis. For the upswing of the driving sinusoid all three dynamical regimes are displayed: from the node in regimes II and III (blue in Fig. 2), through epileptiform dynamics in regime IV (continuous red in Fig. 2), to alpha oscillations in regime V (green in Fig. 2). During the downswing phase of the driving, however, the system remains in quasistatic conditions in the alpha attractor, so in the bistable regimes IV and III it exhibits alpha oscillations (green in Fig. 2) and in the bistable regime II it remains on the focus (cyan in Fig. 2). This hysteresis loop is closed when driving with a sufficiently high amplitude moves the system to, or sufficiently close, regime I, where the system relaxes to the node (blue in Fig. 2). This effect occurs in regimes “c” and “i” combining all three types of dynamics. An exemplary time course corresponding to regime “c” is provided in Supplementary Materials, in Fig. S9. For smaller driving frequencies the system remains in alpha oscillations and does not revert to the node (regime “d”). A similar effect is observed for initial conditions set to the focus (panel Fig. 6B). These effects explain why stochastic driving with power concentrated in low frequencies promotes alpha oscillations of the system (as described in section 3.1). Supplementary Materials, Fig. S10 shows

how slow driving, characterised with a sufficiently high amplitude, pushes the system deeper into the alpha limit cycle, thereby increasing the amplitude of alpha oscillations. We note that these model regimes are also physiologically relevant, since slow (0.25Hz) driving has been shown to lead to an increased power in the α band [61, 45] and bursting following a slow quasi-harmonic pattern may occur in the early ictal phase of seizures [62].

4. Discussion

In this study we investigated the effect of rhythmic driving and coloured noise on the generation of epileptiform dynamics in a neural mass model. We found that epileptiform dynamics are more readily elicited by noise with certain temporal correlations. By exploring the composition of OU noise in different frequency bands and driving of the model with sinusoidal rhythms, we discovered that simulated epileptiform discharges are more easily generated by rhythms in the delta and theta frequency bands. Thus we suggest that the local microcircuit interactions embodied by the model can give rise to emergent dynamics that leave it prone to generating epileptiform rhythms when bombarded by afferent spiking with particular rhythmic properties.

Experimental and clinical findings lend support to this hypothesis. Interictal focal slow activity in the delta or delta-theta bands has been shown to be present in a majority of invasive recordings from people with temporal lobe epilepsy [32], and it lateralises with regions of seizure onset [32], in particular in neocortical temporal lobe epilepsy [36]. Thus slow rhythms are associated with epileptic brain networks [36]. Our modelling results lead us to hypothesise that such rhythms could also be the cause of onset of seizures in such networks. Indeed, slow rhythms are also observed in invasive recordings at seizure onset in focal epilepsies [37, 63]. Slow rhythms have also been observed in association with generalised epilepsies in both clinical and experimental data. [38] observed an increase of delta activity prior to onset of spike-wave-discharges in the WAG/Rij rodent model and [39] reported an increase of delta and theta rhythms in the

preictal phase of brain activity in the same animal model. The frequency of the alpha rhythm has also been shown to be lower in people with epilepsy compared to control subjects [64]. Our results suggest a potential mechanism of propagation of abnormal dynamics in large-scale brain networks: a local network
380 generating abnormal rhythms could induce the propagation of this activity in connected brain regions. Future extensions to our work could examine explicitly the dynamics of networks of neural masses in order to investigate conditions for propagation or restriction of epileptiform activity.

The epileptic brain is increasingly being thought of and studied in terms of
385 networks [65, 10, 8, 12, 66, 67]. Understanding seizure generation in networks is a difficult task since seizures represent emergent transitions in dynamics due to both the underlying connectivity structure of the network and the intrinsic dynamics of individual nodes [11, 13]. To simplify this situation, in our study we separated intrinsic node and network effects, considering the effects
390 of temporally structured afferent activity to a node. Our observations that certain rhythms preferably generate epileptiform dynamics arise from an interplay between the presence of different invariant sets (Fig. 2) and the time scale of fluctuations in I_{ex} . For example, on the node branch, close to the epileptiform limit cycle, slow variations in afferents can allow the epileptiform limit-cycle
395 to appear and, if the amplitude of these fluctuations is in a certain interval, the system can also converge to this attractor, therefore displaying epileptiform rhythms. By uncovering these phenomena in the deterministic system, we are able to better understand the ways in which stochastic fluctuations with power in certain frequencies could cause transitions in dynamics and ultimately lead
400 to epileptiform activity.

In our study we used a set of parameters for the Jansen-Rit model that give rise to dynamics relevant to the study of healthy brain function such as the alpha rhythm as well as pathological dynamics [48, 49, 50]. Previous studies have used bifurcation analyses to demonstrate how the arrangement of invariant sets varies
405 in parameter space [58, 27], and have studied the response of neural mass models to driving by rhythmic pulses [46] and white noise [50]. Our work advances

on these previous studies by quantifying the effect that temporally correlated noise and rhythmic input have in terms of the generation of epileptiform spiking, which led us to hypothesise a role for low-frequency brain rhythms in the generation of seizures. We therefore demonstrated the importance of non-white
410 noise in the context of bifurcations of neural mass models to uncover the mechanisms underlying brain (dys-)function. In modelling a complex system such as the brain, a model is only useful so far as it recreates a relevant feature of the dynamics of interest, which here is the presence of epileptiform dynamics. The
415 chosen parameter set enabled us to study the effect that different afferent dynamics have on the generation of these dynamics, and we further demonstrated that variations in the arrangement of attractors did not affect the optimal time scale for induction of epileptiform dynamics.

Our study utilised a neural mass model that is capable of generating epileptiform dynamics via a SNIC bifurcation, which has been shown to be a generic
420 onset mechanism for a variety of epileptiform rhythms, including spike-wave discharges and focal seizures [68, 69]. We therefore believe our results to be applicable in the context of both focal and generalised epilepsies. In future work it will be important to study the effects of coloured noise in a variety of different
425 models, such as extensions to the neural mass model [17, 10] that can generate alternative dynamics, networks of neural masses, or networks of canonical models [18, 70, 22, 69]. It will be interesting to ascertain, for example, the conditions for propagation or restriction of epileptiform activity or whether certain epilepsies with specific emergent dynamics are susceptible to specific afferent
430 rhythms for the generation of seizures.

5. Conclusion

The mechanisms underpinning the generation of seizures are imperfectly understood. In this work we have shown that the temporal correlation of signals afferent to neuronal populations may play a critical role in the initiation of
435 epileptiform dynamics. The reasons for this can be understood in terms of the

dynamical properties of these populations, in particular from the arrangement in parameter space of a variety of dynamical regimes. We therefore highlight the necessity of moving beyond white noise driving in computational studies of epilepsy.

440 6. Acknowledgements

This work was supported by the European Commission through the FP7 Marie Curie Initial Training Network 289146 (NETT: Neural Engineering Transformative Technologies), by the Spanish Ministry of Economy and Competitiveness and FEDER (project FIS2012-37655-C02-01). J.G.O. also acknowledges support from the ICREA Academia programme, the Generalitat de Catalunya (project 2014SGR0947), and the “María de Maeztu” Programme for Units of Excellence in R&D (Spanish Ministry of Economy and Competitiveness, MDM-2014-0370) M.G. gratefully acknowledges the financial support of the EPSRC via grant EP/N014391/1. The contribution of M.G. was generously supported
450 by a Wellcome Trust Institutional Strategic Support Award (WT105618MA).

References

- [1] W. W. Lytton, Computer modelling of epilepsy, *Nature Reviews Neuroscience* 9 (2008) 626–637.
- [2] F. Wendling, P. Benquet, F. Bartolomei, V. Jirsa, Computational models of epileptiform activity, *Journal of Neuroscience Methods* (2015) 1–19.
455
- [3] A. Valentín, G. Alarcón, M. Honavar, J. J. García Seoane, R. P. Selway, C. E. Polkey, C. D. Binnie, Single pulse electrical stimulation for identification of structural abnormalities and prediction of seizure outcome after epilepsy surgery: a prospective study., *Lancet neurology* 4 (2005) 718–26.
- [4] G. R. Iannotti, F. Grouiller, M. Centeno, D. W. Carmichael, E. Abela, R. Wiest, C. Korff, M. Seeck, C. Michel, F. Pittau, S. Vulliemoz, Epileptic
460

networks are strongly connected with and without the effects of interictal discharges, *Epilepsia* (2016) 1–11.

- 465 [5] J. O’Muircheartaigh, C. Vollmar, G. J. Barker, V. Kumari, M. R. Symms, P. Thompson, J. S. Duncan, M. J. Koepp, M. P. Richardson, Abnormal thalamocortical structural and functional connectivity in juvenile myoclonic epilepsy, *Brain* 135 (2012) 3635–3644.
- [6] S. S. Spencer, Neural networks in human epilepsy: evidence of and implications for treatment., *Epilepsia* 43 (2002) 219–27.
- 470 [7] M. a. Kramer, S. S. Cash, Epilepsy as a Disorder of Cortical Network Organization, *The Neuroscientist* 18 (2012) 360–372.
- [8] M. P. Richardson, Large scale brain models of epilepsy: dynamics meets connectomics., *Journal of neurology, neurosurgery, and psychiatry* (2012).
- [9] E. van Diessen, S. J. H. Diederens, K. P. J. Braun, F. E. Jansen, C. J. Stam, Functional and structural brain networks in epilepsy: what have we learned?, *Epilepsia* 54 (2013) 1855–65.
- 475 [10] M. Goodfellow, K. Schindler, G. Baier, Intermittent spike-wave dynamics in a heterogeneous, spatially extended neural mass model., *NeuroImage* 55 (2011) 920–32.
- 480 [11] J. R. Terry, O. Benjamin, M. P. Richardson, Seizure generation: the role of nodes and networks., *Epilepsia* 53 (2012) e166–9.
- [12] G. Petkov, M. Goodfellow, M. P. Richardson, J. R. Terry, A Critical Role for Network Structure in Seizure Onset: A Computational Modeling Approach, *Frontiers in Neurology* 5 (2014).
- 485 [13] M. T. J. Goodfellow, Estimation of brain network ictogenicity predicts outcome from epilepsy surgery, *Nature Publishing Group* 44 (2016) 1–13.

- [14] T. I. Aksenova, V. V. Volkovich, A. E. P. Villa, Detection of spectral instability in EEG recordings during the preictal period, *Journal of Neural Engineering* 4 (2007) 173–178.
- 490 [15] A. E. P. Villa, I. V. Tetko, Cross-frequency coupling in mesiotemporal EEG recordings of epileptic patients, *Journal of Physiology Paris* 104 (2010) 197–202.
- [16] P. Suffczynski, F. Wendung, J. J. Bellanger, F. H. L. Da Silva, Some insights into computational models of (patho)physiological brain activity, 495 *Proceedings of the IEEE* 94 (2006) 784–804.
- [17] F. Wendling, F. Bartolomei, J. J. Bellanger, P. Chauvel, Epileptic fast activity can be explained by a model of impaired GABAergic dendritic inhibition, *European Journal of Neuroscience* 15 (2002) 1499–1508.
- [18] F. H. Lopes da Silva, W. Blanes, S. N. Kalitzin, J. Parra, P. Suffczynski, D. N. Velis, Dynamical diseases of brain systems: different routes to epileptic seizures., *IEEE transactions on bio-medical engineering* 50 (2003) 540–8. 500
- [19] M. Breakspear, J. A. Roberts, J. R. Terry, S. Rodrigues, A Unifying Explanation of Primary Generalized Seizures Through Nonlinear Brain Modeling and Bifurcation Analysis (2006). 505
- [20] A. Rothkegel, K. Lehnertz, Recurrent events of synchrony in complex networks of pulse-coupled oscillators, *EPL (Europhysics Letters)* 95 (2011) 38001.
- [21] G. Baier, M. Goodfellow, P. N. Taylor, Y. Wang, D. J. Garry, The importance of modeling epileptic seizure dynamics as spatio-temporal patterns., 510 *Frontiers in physiology* 3 (2012) 281.
- [22] M. Goodfellow, P. Glendinning, Mechanisms of intermittent state transitions in a coupled heterogeneous oscillator model of epilepsy., *Journal of mathematical neuroscience* 3 (2013) 17.

- 515 [23] F. H. Lopes da Silva, A. Hoeks, H. Smits, L. H. Zetterberg, Model of brain rhythmic activity, *Kybernetik* 15 (1974) 27–37.
- [24] A. J. Pons, J. L. Cantero, M. Atienza, J. Garcia-Ojalvo, Relating structural and functional anomalous connectivity in the aging brain via neural mass modeling., *NeuroImage* 52 (2010) 848–61.
- 520 [25] J. D. Victor, J. D. Drover, M. M. Conte, N. D. Schiff, Mean-field modeling of thalamocortical dynamics and a model-driven approach to EEG analysis., *Proceedings of the National Academy of Sciences of the United States of America* 108 Suppl (2011) 15631–8.
- [26] J. a. Roberts, P. a. Robinson, Quantitative theory of driven nonlinear brain dynamics, *NeuroImage* 62 (2012) 1947–1955.
- 525 [27] J. Touboul, F. Wendling, P. Chauvel, O. Faugeras, Neural Mass Activity, Bifurcations, and Epilepsy, *Neural computation* 23 (2011) 3232–86.
- [28] A. Garnier, A. Vidal, C. Huneau, H. Benali, A neural mass model with direct and indirect excitatory feedback loops: identification of bifurcations and temporal dynamics., *Neural computation* 27 (2015) 329–64.
- 530 [29] G. Buzsáki, A. Draguhn, Neuronal oscillations in cortical networks., *Science (New York, N.Y.)* 304 (2004) 1926–9.
- [30] E. Niedermeyer, F. H. Lopes da Silva, *Electroencephalography: basic principles, clinical applications, and related fields*, Lippincott Williams and Wilkins, Philadelphia, 5th ed edition, 2005.
- 535 [31] W. J. Freeman, L. J. Rogers, M. D. Holmes, D. L. Silbergeld, Spatial spectral analysis of human electrocorticograms including the alpha and gamma bands., *Journal of neuroscience methods* 95 (2000) 111–21.
- [32] A. Valentín, G. Alarcón, S. F. Barrington, J. J. García Seoane, M. C. Martín-Miguel, R. P. Selway, M. Koutroumanidis, Interictal estimation of
- 540

intracranial seizure onset in temporal lobe epilepsy, *Clinical Neurophysiology* 125 (2014) 231–238.

- [33] P. J. Karoly, D. R. Freestone, R. Boston, D. B. Grayden, D. Himes, K. Leyde, U. Seneviratne, S. Berkovic, T. O'Brien, M. J. Cook, Interictal spikes and epileptic seizures: Their relationship and underlying rhythmicity, *Brain* 139 (2016) 1066–1078.
- [34] D. Gupta, P. Ossenblok, G. van Luijtelaar, Space-time network connectivity and cortical activations preceding spike wave discharges in human absence epilepsy: a MEG study, *Med Biol Eng Comput* 49 (2011) 555–565.
- [35] L. G. Sadleir, K. Farrell, S. Smith, M. B. Connolly, I. E. Scheffer, Electroclinical features of absence seizures in sleep, *Epilepsy Research* 93 (2011) 216–220.
- [36] J. X. Tao, X. J. Chen, M. Baldwin, I. Yung, S. Rose, D. Frim, S. Hawes-Ebersole, J. S. Ebersole, Interictal regional delta slowing is an EEG marker of epileptic network in temporal lobe epilepsy, *Epilepsia* 52 (2011) 467–476.
- [37] S.-A. Lee, D. D. Spencer, S. S. Spencer, Intracranial eeg seizure-onset patterns in neocortical epilepsy, *Epilepsia* 41 (2000) 297–307.
- [38] E. Sitnikova, G. van Luijtelaar, Electroencephalographic precursors of spike-wave discharges in a genetic rat model of absence epilepsy: Power spectrum and coherence EEG analyses, *Epilepsy Research* 84 (2009) 159–171.
- [39] G. Van Luijtelaar, A. Hramov, E. Sitnikova, A. Koronovskii, Spike-wave discharges in WAG/Rij rats are preceded by delta and theta precursor activity in cortex and thalamus, *Clinical Neurophysiology* 122 (2011) 687–695.
- [40] A. Destexhe, M. Rudolph, Extracting information from the power spectrum of synaptic noise., *Journal of computational neuroscience* 17 (2004) 327–45.

- [41] W. Braun, P. C. Matthews, R. Thul, First-passage times in integrate-
and-fire neurons with stochastic thresholds, *Physical Review E* 91 (2015)
570 1–7.
- [42] L. a. da Silva, R. D. Vilela, Colored noise and memory effects on formal
spiking neuron models, *Physical Review E* 91 (2015) 062702.
- [43] F. Freyer, J. A. Roberts, R. Becker, P. A. Robinson, P. Ritter, M. Break-
575 spear, Biophysical Mechanisms of Multistability in Resting-State Cortical
Rhythms, *The Journal of Neuroscience* 31 (2011) 6353–6361.
- [44] B. Sancristóbal, R. Vicente, J. M. Sancho, J. Garcia-Ojalvo, Emergent
bimodal firing patterns implement different encoding strategies during
gamma-band oscillations., *Frontiers in computational neuroscience* 7 (2013)
580 18.
- [45] M. Jedynak, A. J. Pons, J. Garcia-Ojalvo, Cross-frequency transfer in a
stochastically driven mesoscopic neuronal model, *Frontiers in Computa-
tional Neuroscience* 9 (2015) 1–12.
- [46] A. Spiegler, T. R. Knösche, K. Schwab, J. Haueisen, F. M. Atay, Modeling
585 brain resonance phenomena using a neural mass model., *PLoS computa-
tional biology* 7 (2011) e1002298.
- [47] D. Malagarriga, A. E. P. Villa, J. Garcia-Ojalvo, A. J. Pons, Mesoscopic
Segregation of Excitation and Inhibition in a Brain Network Model, *PLoS
Computational Biology* 11 (2015) 1–21.
- 590 [48] B. H. Jansen, G. Zouridakis, M. E. Brandt, A neurophysiologically-based
mathematical model of flash visual evoked potentials, *Biological Cybernetics*
68 (1993) 275–283.
- [49] B. H. Jansen, V. G. Rit, Electroencephalogram and visual evoked potential
595 generation in a mathematical model of coupled cortical columns, *Biological
Cybernetics* 73 (1995) 357–366.

- [50] F. Wendling, J. J. Bellanger, F. Bartolomei, P. Chauvel, Relevance of nonlinear lumped-parameter models in the analysis of depth-EEG epileptic signals., *Biological cybernetics* 83 (2000) 367–78.
- [51] F. Grimbert, O. Faugeras, Bifurcation analysis of Jansen’s neural mass model., *Neural computation* 18 (2006) 3052–68.
- [52] H. R. Wilson, J. D. Cowan, Excitatory and inhibitory interactions in localized populations of model neurons., *Biophysical journal* 12 (1972) 1–24.
- [53] W. J. Freeman, Linear analysis of the dynamics of neural masses., *Annual review of biophysics and bioengineering* 1 (1972) 225–56.
- [54] S. Amari, Homogeneous nets of neuron-like elements, *Biological Cybernetics* 17 (1974) 211220.
- [55] P. Nunez, The brain wave equation: a model for the EEG, *Mathematical Biosciences* 291 (1974) 279–297.
- [56] B. Ermentrout, *Simulating, analyzing, and animating dynamical systems : a guide to XPPAUT for researchers and students*, Philadelphia, Society for Industrial and Applied Mathematics, 2002.
- [57] G. J. L. Carlo Laing, *Stochastic Methods in Neuroscience*, Oxford University Press, 2010.
- [58] A. Spiegler, S. J. Kiebel, F. M. Atay, T. R. Knösche, Bifurcation analysis of neural mass models: Impact of extrinsic inputs and dendritic time constants., *NeuroImage* 52 (2010) 1041–58.
- [59] M. a. Kramer, W. Truccolo, U. T. Eden, K. Q. Lepage, L. R. Hochberg, E. N. Eskandar, J. R. Madsen, J. W. Lee, A. Maheshwari, E. Halgren, C. J. Chu, S. S. Cash, Human seizures self-terminate across spatial scales via a critical transition, *Proceedings of the National Academy of Sciences* 109 (2012) 21116–21121.
- [60] R. Toral, P. Colet, *Stochastic Numerical Methods*, Wiley-VCH, 2014.

- [61] L. Bayer, I. Constantinescu, S. Perrig, J. Vienne, P.-P. Vidal, M. Mühlethaler, S. Schwartz, Rocking synchronizes brain waves during a short nap., *Current biology : CB* 21 (2011) R461–2.
- [62] G. Alarcon, C. D. Binnie, R. D. Elwes, C. E. Polkey, Power spectrum and intracranial EEG patterns at seizure onset in partial epilepsy., *Electroencephalography and clinical neurophysiology* 94 (1995) 326–337.
- [63] D. Jiménez-Jiménez, R. Nekkare, L. Flores, K. Chatzidimou, I. Bodi, M. Honavar, N. Mullatti, R. D. Elwes, R. P. Selway, A. Valentín, G. Alarcón, Prognostic value of intracranial seizure onset patterns for surgical outcome of the treatment of epilepsy, *Clinical Neurophysiology* 126 (2015) 257 – 267.
- [64] P. G. Larsson, H. Kostov, Lower frequency variability in the alpha activity in EEG among patients with epilepsy, *Clinical Neurophysiology* 116 (2005) 2701–2706.
- [65] A. T. Berg, S. F. Berkovic, M. J. Brodie, J. Buchhalter, J. H. Cross, W. Van Emde Boas, J. Engel, J. French, T. a. Glauser, G. W. Mathern, S. L. Moshé, D. Nordli, P. Plouin, I. E. Scheffer, Revised terminology and concepts for organization of seizures and epilepsies: Report of the ILAE Commission on Classification and Terminology, 2005-2009, *Epilepsia* 51 (2010) 676–685.
- [66] P. Sanz-Leon, S. A. Knock, A. Spiegler, V. K. Jirsa, Mathematical framework for large-scale brain network modeling in The Virtual Brain, *NeuroImage* 111 (2015) 385–430.
- [67] S. Naze, C. Bernard, V. Jirsa, Computational Modeling of Seizure Dynamics Using Coupled Neuronal Networks: Factors Shaping Epileptiform Activity, *PLOS Computational Biology* 11 (2015) e1004209.
- [68] F. Marten, S. Rodrigues, O. Benjamin, M. P. Richardson, J. R. Terry, Onset of polyspike complexes in a mean-field model of human electroencephalography and its application to absence epilepsy., *Philosophical transactions.*

Series A, Mathematical, physical, and engineering sciences 367 (2009) 1145–61.

[69] V. K. Jirsa, W. C. Stacey, P. P. Quilichini, A. I. Ivanov, C. Bernard, On the nature of seizure dynamics., *Brain : a journal of neurology* (2014) 2210–2230.
655

[70] O. Benjamin, T. H. Fitzgerald, P. Ashwin, K. Tsaneva-Atanasova, F. Chowdhury, M. P. Richardson, J. R. Terry, A phenomenological model of seizure initiation suggests network structure may explain seizure frequency in idiopathic generalised epilepsy., *Journal of mathematical neuroscience* 2 (2012) 1.
660

Accepted manuscript